University of Amsterdam
Research Master Brain and Cognitive Sciences

Project Report: Neural dynamics and Deep Learning

Mechanisms of distributed working memory in a large-scale network of macaque neocortex

28/11/2022 - 22/12/2022

Student:
Paolo Umberto Agliati
13978926

Supervisor:
Jorge Mejias

Group:
Violeta Céspedes, Paolo Umberto Agliati, Rosa Großmann

Contents

1 Introduction **2**

2 Methods **2**

3 Replication Results **2**

4 Individual Expansion: AMPA **4**
4.1 Introduction 4
4.2 Methods 4
4.3 Results 5
4.4 Discussion 12

5 References **13**

1 Introduction

Working Memory (WM) can be defined as the short-term storage and manipulation of sensory information that can be retained, in the absence of external stimuli, for some seconds (Baddeley et al., 2003). The phenomenon has been widely studied for its clinical implications (Morey et al., 2009; Nakao et al., 2009) as well as for its prevalent role in cognitive functions such as perception, decision-making, and action control (Curtis and Lee, 2010; Kang et al.,2011; Baddeley et al., 2001). Mejías and Wang (2022) developed a large-scale computational model that embedded experimentally-derived biophysical properties to examine the dynamics of working memory implementation and propagation in the macaque brain, in order to gain insight into the mechanisms of distributed working memory.

2 Methods

In this project, we replicated the model built by Mejias and Wang (2022). It is a large-scale model of 30 areas across all four neocortical lobes. For each area, a local model describes the temporal evolution of firing rates of three populations - two input-specific excitatory populations and one inhibitory population. The local connectivity, described in detail in the Method section of the original paper, creates a winner-takes-all dynamic which allows only one of the two excitatory populations (namely, the one that receives an input) to show an increased firing rate. The evolution of the firing rates of each population can be described by Equation 1, in which A and B are the two excitatory populations, and C refers to the inhibitory population.

$$\begin{aligned} \frac{dS_A}{dt} &= \frac{-S_A}{\tau_N} + \gamma(1 - S_A)\, r_A \\ \frac{dS_B}{dt} &= \frac{-S_B}{\tau_N} + \gamma(1 - S_B)\, r_B \\ \frac{dS_C}{dt} &= \frac{-S_C}{\tau_G} + \gamma_I\, r_C \end{aligned} \tag{1}$$

The first two equations describe how the firing rate in the excitatory populations change over time, whereas the third equation describes the change of the firing rate of the inhibitory population. This yields for every area of the model. S represents the conductances, r the firing rates, τ the time constants, and γ is a constant. The entire large-scale model comprises 30 of the above described local circuits, simulating the 30 different areas. Additionally, the strength of inter areal projections is scaled according to data from research on the connectivity of the macaque neocortex (Elston, 2007), and feedback inhibition coming from areas higher in the cortical hierarchy as defined by anatomical studies (Felleman and Van Essen, 1991; Markov et al., 2014a) is implemented by strengthening their projections towards the areas lower in the hierarchy.

3 Replication Results

We successfully replicated the model by Mejias and Wang (2022) and produced results that are identical with figures 2C and 2D, as well as figure 4D from the original paper. In the replication of figure 2C (Fig. 1) it is visible that an input of 0.5s in V1 leads to an increased persistent firing rate in displayed areas LIP, 24c, 2, and 9/46d. This shows that the areas are properly connected via long-range synapses.

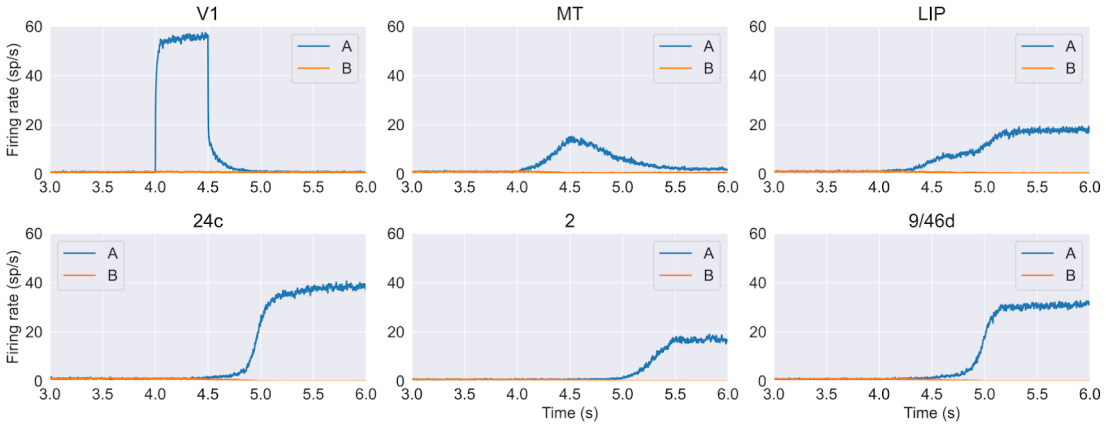

Figure 1: Simulation of response in selected areas during a working memory task. Input in excitatory population A in V1. Replication of figure 2C in Mejias et al. (2022).

Furthermore, the heterogeneity of the areas, meaning the different strengths of inter areal connections, is shown in the replication of figure 2D (see Fig. 2). Low level areas have a lower firing rate during the delay period (after the input is withdrawn), compared to the higher level.

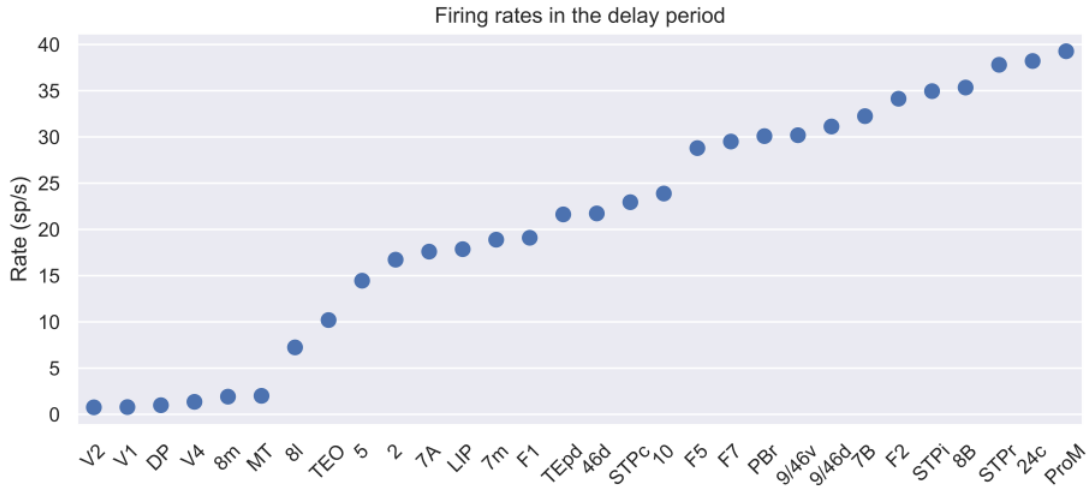

Figure 2: Firing rate of all areas in the delay period. Replication of figure 2D in Mejias et al.(2022).

The counterstream inhibitory bias (CIB) introduces feedback inhibition into the model, leading to a more distinct firing rate pattern among the areas in the delay period. This can be observed in Fig. 3 (replication of figure 4D).

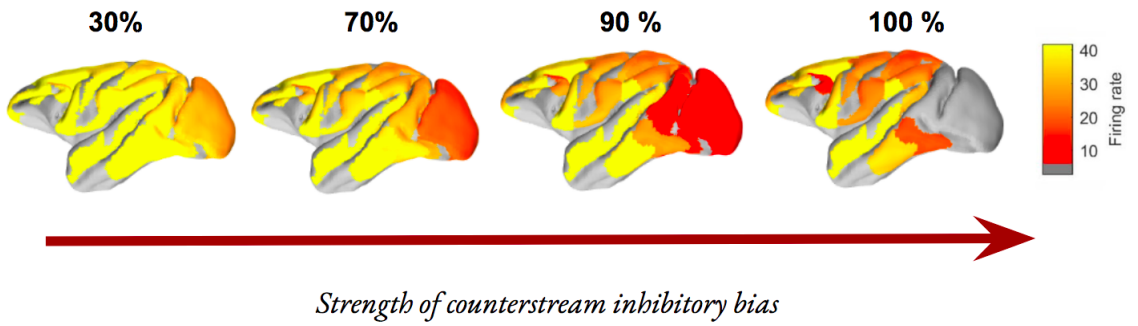

Figure 3: Firing rate across all modeled areas with different strengths of CIB. Replication of figure 4D in Mejias et al. (2022).

4 Individual Expansion: AMPA

4.1 Introduction

For this expansion on the work of Mejías and Wang, AMPA receptors (AMPAR) will be introduced in the model. AMPARs are glutamatergic channels widely present in excitatory neurons. Although they share the same selectivity, they have a significantly simpler mechanism of functioning when compared to the already implemented NMDA receptors, and show quicker kinetics of opening and closure. AMPARs are believed to be implicated in signal propagation, a feature that plays a big role in interareal phenomena such as WM (Van Vugt et al., 2020). Furthermore, the study of AMPA/NMDA couplings can have clinical implications since their levels are found to be altered with the introduction of drugs (Simoes et al., 2007). In this extension, we will address two main questions: What's the role of AMPA in signal propagation? What is the contribution of AMPA in the system's bistability (and therefore in its ability to remember information)?

4.2 Methods

In order to implement AMPA in the system, the value of AMPA coupling needs to be introduced. This will mainly affect the equations describing the input dynamics of each area (see Equation 2).

$$\begin{aligned} I_A &= J_S S_A + J_C S_B + J_E I S_c + I_0 A + I^A_{net} + x_A\,(t) \\ I_B &= J_S S_A + J_C S_B + J_E I S_c + I_0 B + I^B_{net} + x_B\,(t) \\ I_C &= J_I E S_A + J_I E S_B + J_I I S_c + I_0 C + I^C_{net} + x_C\,(t) \end{aligned} \tag{2}$$

These equations describe the coupling effects on Input strength: the parameters J_s, J_c, and $J_E I$ are matrices describing the coupling strength of receptors in the excitatory populations. Values of coupling for AMPARs were introduced in these parameters.

Additionally, to study the differential effects of AMPA coupling strengths, the global parameter A is introduced, which scales the coupling of AMPA in all areas, for all excitatory populations. Similarly, we introduce another parameter N, to scale the coupling strengths of NMDA receptors.

We then want to quantify the contribution of AMPA in signal propagation, and to do so we will focus on two main aspects: the mean firing rates of the persistent activity period (last second of the simulation) which we will refer to as Rf, and the rising time (rT), defined in Fig. 4.

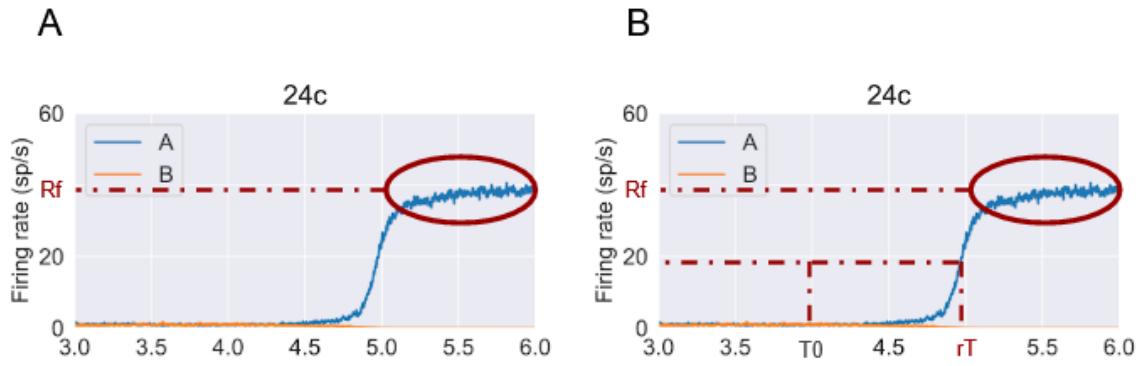

Figure 4: Example of defining Rf as the mean firing rate of the persistent activity period for area 24C (A). Example of defining rT in the same area, we consider the time corresponding to Rf/2, measured starting from T0=4s, the time in which the input is given to the system (B).

4.3 Results

The initial observations on the model after the introduction of AMPARs are what drove the subsequent analyses on firing rates and stimulus propagation. These constituted simple inspection of the changes in the firing rate over time graphs when the value of parameter A is increased (see Fig. 5).

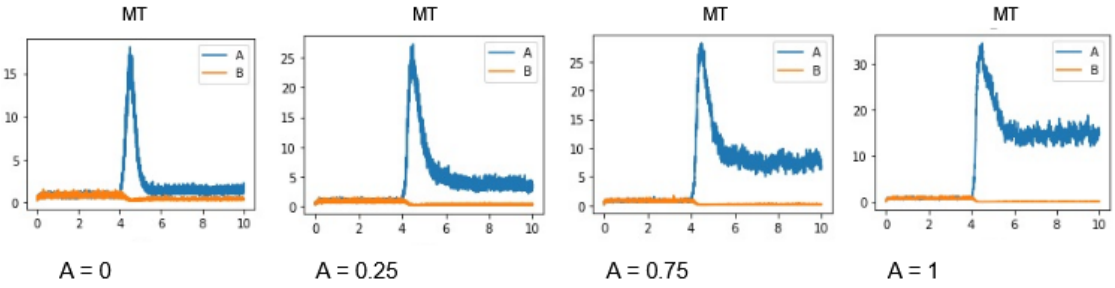

Figure 5: Example of changes in firing rate over time for different strengths of AMPA coupling for area MT. The level of sustained activity during the last seconds of the simulation and the slope of the rising part of the curve are the most evident changes when increasing the parameter A.

Investigation 1

We first focus on the effects of AMPA on the delay period. Previous studies showed how AMPA activity in macaques affects WM by changing the firing rates of this sustained activity period in cortical areas (Van Vugt et al., 2020). Therefore, we first measure the mean firing rates of the last second of the simulations, running them for different strengths of AMPA and NMDA coupling. In Fig. 6, such measure is averaged across all areas, to get a bird's eye view of the behavior of the whole system in these different conditions.

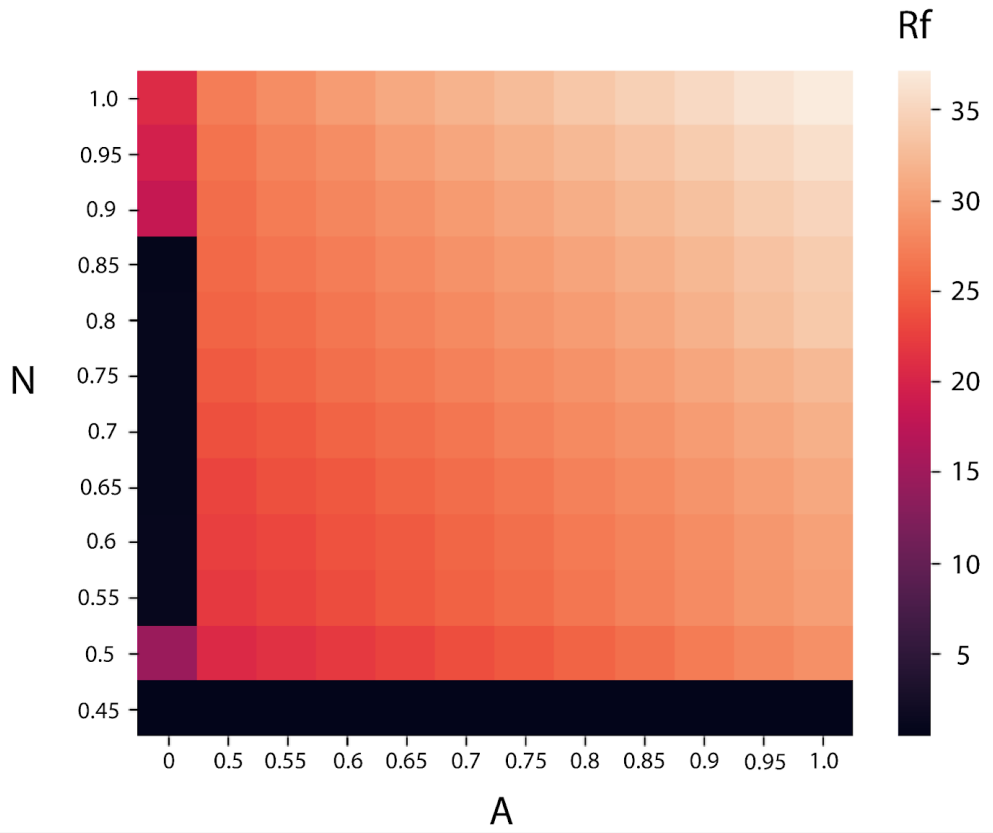

Figure 6: Changes in the firing rates of the persistent activity period (Rf) for different values of coupling strengths of AMPA and NMDA (parameters A and N), averaged across all areas.

In this case, it is evident how increasing the coupling of AMPA and NMDA progressively increases the firing rates of the persistent activity period in the system as a whole, highlighting the role of AMPA in the propagation of the signal. The effects of AMPA on the delay period can also be observed in an area-specific way, as seen in Fig. 7. The three areas in the bottom row are the later areas in the visual hierarchy, they receive the input stimulus from earlier areas and initiate the persistent activity associated with WM. In these areas, increasing the coupling of both receptors will again cause an incremental raise in Rf. The top three areas are early areas in the visual hierarchy and reflect the function of propagating the visual stimulus to later, more frontal areas. Interestingly, the profile changes for these areas, since the highest Rf seems to be achieved by different combinations of N and A than the maximum one. This illustrates the effect of feedback inhibition (implemented via CIB) in the system, as increasing NMDA coupling over a certain value will also increase the magnitude of the inhibition from frontal areas and cause Rf to decline. Even in those cases, we can still see how the effect of a higher AMPA coupling is always to increase the signal transmission by raising the firing rates in the delay period.

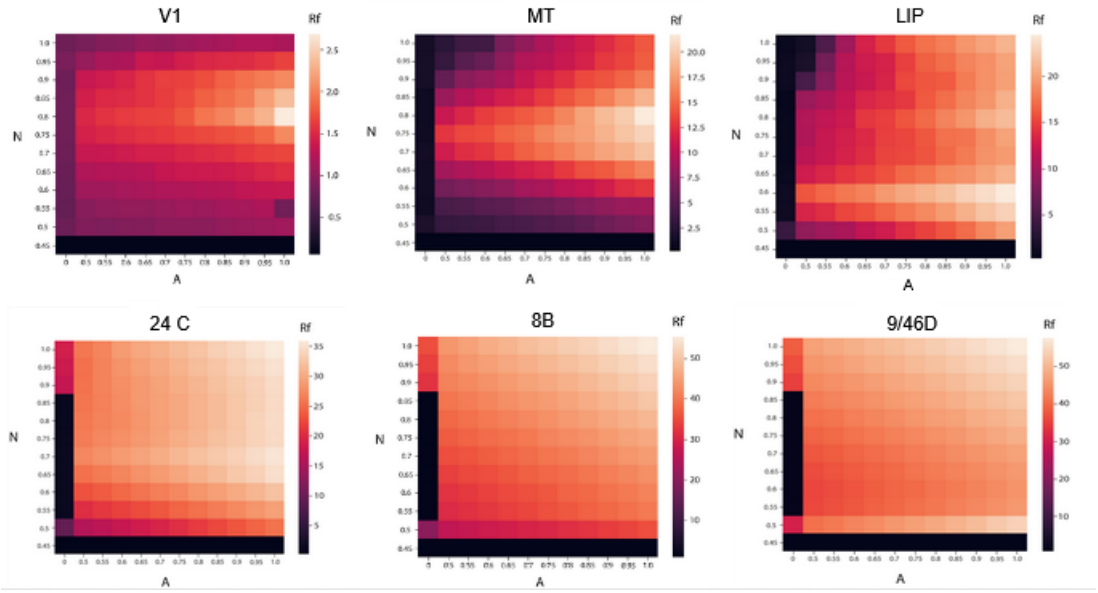

Figure 7: Changes in the firing rates of the persistent activity period (Rf) for different values of coupling strengths of AMPA and NMDA (parameters A and N), for 6 different areas.

Investigation 2

We then consider the effect of AMPA coupling on the rising time (rT), to get an indication of how fast the firing rates increase after the input is given to the system. Once again, we will measure the value of rT for different combinations of A and N, both considering the global averages and the area-specific cases. As can be seen in Fig. 8, considering all areas will give the general indication that the rising time gets progressively shorter with the increase in AMPA coupling. A similar pattern is repeated in Fig. 9 for higher areas in the hierarchy (bottom row), and the same tendency can be seen for somatosensory area 2. As for Rf, also rTs in earlier visual areas lose this tendency, and show more noisy patterns (as is the case for LIP). In specific cases, for instance for area MT, they display a pattern that seems to follow the one in Fig. 7 but in reverse, therefore showing higher rTs for higher levels of A.

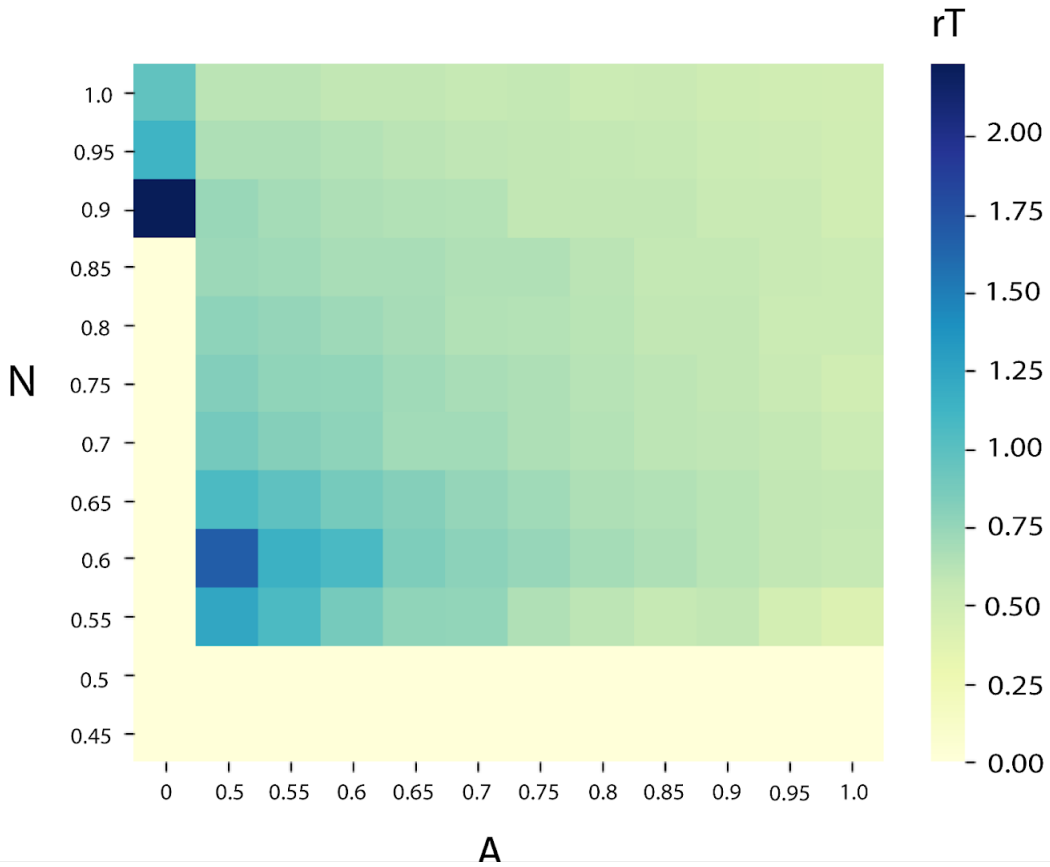

Figure 8: Changes in the rising time (rT) for different values of coupling strengths of AMPA and NMDA (parameters A and N), averaged across all areas.

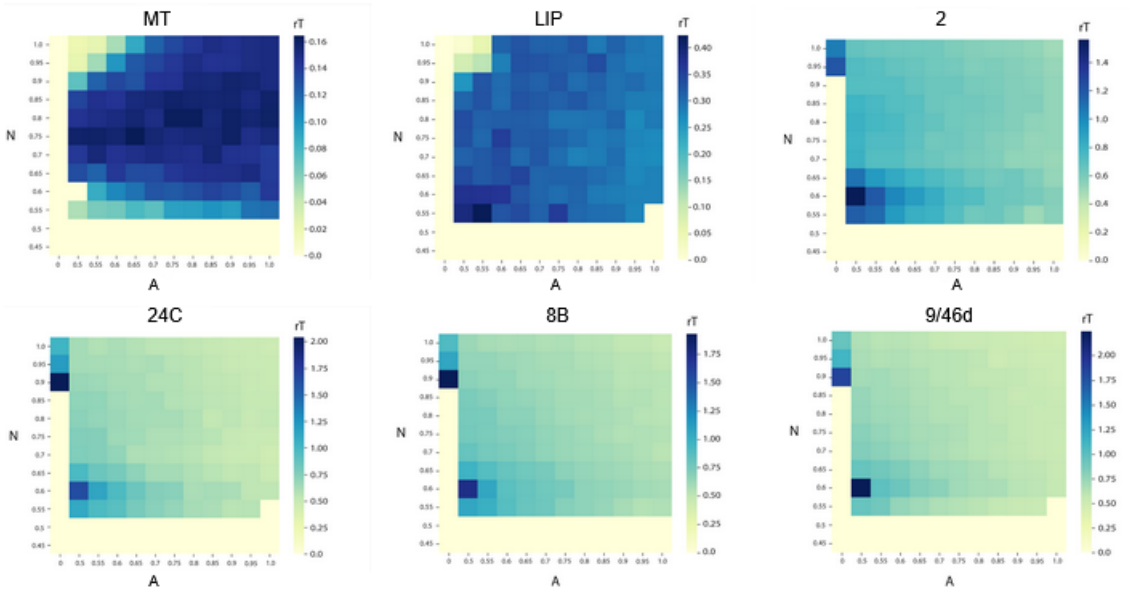

Figure 9: Changes in the rising time (rT) for different values of coupling strengths of AMPA and NMDA (parameters A and N), for 6 different areas.

These tendencies are explained when we consider how rT is defined. The time rT corresponds to a firing rate half of Rf. But since higher AMPA coupling increases Rf, the time corresponding to its half will also be increased. This means that for lower areas in the hierarchy, as A increases the decrease in rising time is overshadowed by the effect of the same increase in A on the firing rates. The effect is illustrated in Fig. 10.

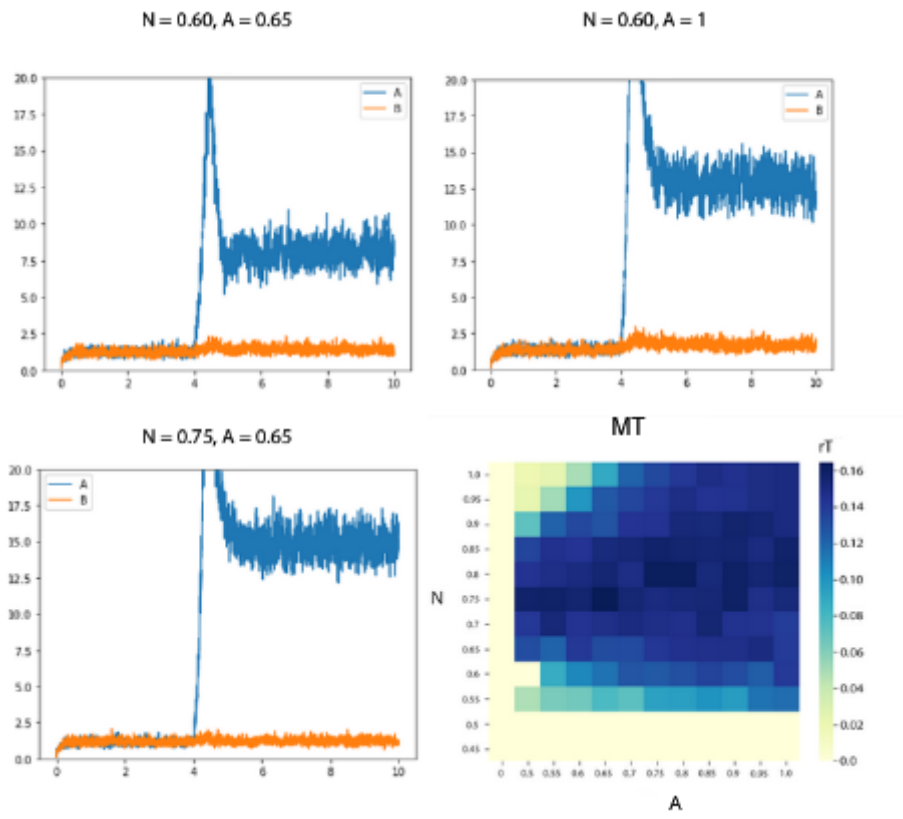

Figure 10: Changes in the rising time (rT) for different values of coupling strengths of AMPA and NMDA (parameters A and N), for area MT. A sufficient increase in any of the parameters will push Rf (and Rf/2, from which rT is derived) to higher values, and will cause rT to shift towards slower times.

Other peculiar effects on rT, as the dark spots observable in higher areas in the hierarchy are explained by the emergence of new shapes in the local firing rate increase, as shown on Fig. 11. Overall, the effect of AMPA on the system seems to be more diverse when considering rT as a measure. This may highlight the need for a different measure of rising time, for instance, some direct measure of the slope of the rate over time curve.

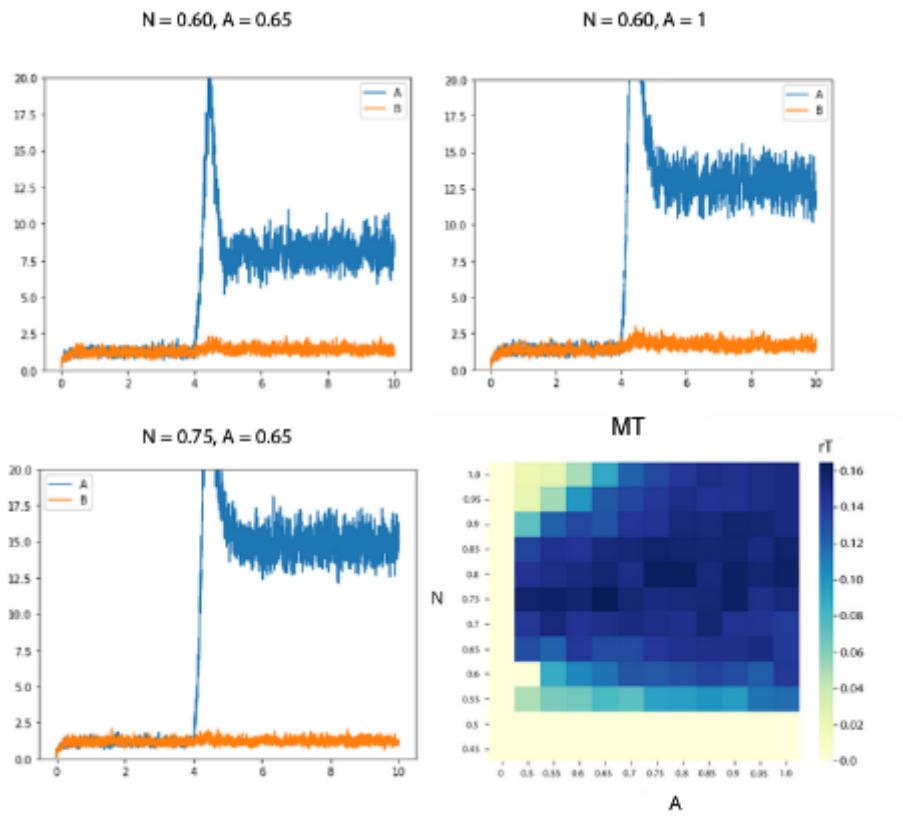

Figure 11: Changes in the rising time (rT) for increasing values of coupling strengths NMDA (parameter N), for area 2. The rise in rT is linked to the emergence of peculiar shapes in the rate over time profile.

Investigation 3

Lastly, we want to directly assess the influence of AMPA on the ability of the system to reach bistability, and therefore to achieve WM. For this investigation, we run simulations for different A and N values, and we assess if the firing rates of relevant areas are increased and if such increase is sustained in time. This profile can be easily deduced by observing the rate over time graphs for all areas and determining the presence of sustained activity. This results in a phase diagram (see Fig. 12) in which the role of AMPA can be linked to the system being bistable, and therefore able to remember the visual input.

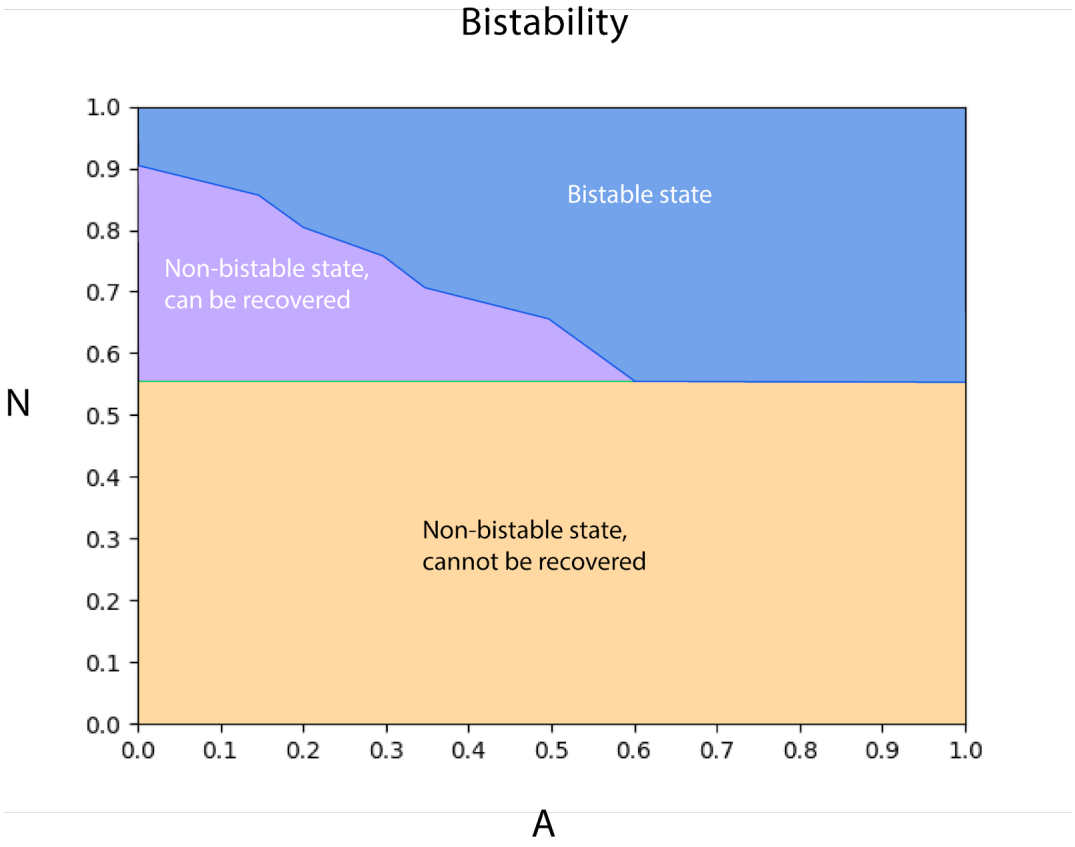

Figure 12: Phase diagram that describes the behavior of the system depending on different values of N and A. In the yellow area, NMDA coupling strength is not enough to give bistability to the system, and no value of A is able to recover such state; in the purple area, the system is not bistable, but increasing AMPA coupling will eventually push it into bistability; in the blue area the system is bistable.

4.4 Discussion

Improvements in the investigations on the introduction of AMPA in the study of WM can be directed towards biological plausibility. The main limiting factor in this regard is the way in which AMPA coupling is introduced since no heterogeneity between areas or biologically informed constraint has been put into the system. Specifically, NMDA coupling strength is modulated in an area-specific manner, through the formation of a gradient, which follows data from the literature in macaques (see Methods section). In order to better assess the effects of AMPA, a gradient for this receptor should be introduced. Furthermore, a lot in this investigation and in the general context of WM is influenced by the timing of transmission of the signal. To better describe this phenomenon in the model, the influence of the physical distance between areas should be taken into consideration. Such distance-dependent timing of transmission cannot be accounted for by just considering slow NMDA kinetics, therefore AMPA can be a significant improvement to the realism of the model.

5 References

Baddeley, A., Chincotta, D., & Adlam, A. (2001). Working memory and the control of action: evidence from task switching. Journal of experimental psychology: General, 130(4), 641.

Curtis, C. E., & Lee, D. (2010). Beyond working memory: the role of persistent activity in decision making. Trends in cognitive sciences, 14(5), 216-222.

Elston, G. N. (2007). Specialization of the neocortical pyramidal cell during primate evolution.

Felleman, D. J., & Van Essen, D. C. (1991). Distributed hierarchical processing in the primate cerebral cortex. Cereb Cortex1: 1–47.

Kang, M. S., Hong, S. W., Blake, R., & Woodman, G. F. (2011). Visual working memory contaminates perception. Psychonomic Bulletin Review, 18(5), 860-869.

Leavitt, M. L., Mendoza-Halliday, D., & Martinez-Trujillo, J. C. (2017). Sustained activity encoding working memories: not fully distributed. Trends in Neurosciences, 40(6), 328-346.

Markov, N. T., Ercsey-Ravasz, M. M., Ribeiro Gomes, A. R., Lamy, C., Magrou, L., Vezoli, J., ...& Kennedy, H. (2014a). A weighted and directed interareal connectivity matrix for macaque cerebral cortex. Cerebral cortex, 24(1), 17-36.

Morey, R. A., Dolcos, F., Petty, C. M., Cooper, D. A., Hayes, J. P., LaBar, K. S., & McCarthy, G. (2009). The role of trauma-related distractors on neural systems for working memory and emotion processing in posttraumatic stress disorder. Journal of psychiatric research, 43(8), 809-817.

Nakao, T., Nakagawa, A., Nakatani, E., Nabeyama, M., Sanematsu, H., Yoshiura, T., ...& Kanba, S. (2009). Working memory dysfunction in obsessive–compulsive disorder: a neuropsychological and functional MRI study. Journal of psychiatric research, 43(8), 784-791.

Simoes, P. F., Silva, A. P., Pereira, F. C., Marques, E., Grade, S., Milhazes, N., ... & Macedo, T. R. (2007). Methamphetamine induces alterations on hippocampal NMDA and AMPA receptor subunit levels and impairs spatial working memory. Neuroscience, 150(2), 433-441.

Van Vugt, B., van Kerkoerle, T., Vartak, D., & Roelfsema, P. R. (2020). The contribution of AMPA and NMDA receptors to persistent firing in the dorsolateral prefrontal cortex in working memory. Journal of Neuroscience, 40(12), 2458-2470.